# Elastic scattering and transfer reactions induced by 100 MeV $^{32}$S on $^{27}$Al†

J. D. Garrett* and H. E. Wegner
*Brookhaven National Laboratory, Upton, New York 11973*

T. M. Cormier, E. R. Cosman, Ole Hansen,* and A. J. Lazzarini
*Department of Physics and Laboratory for Nuclear Science, Massachusetts Institute of Technology, Cambridge, Massachusetts 02139*

(Received 17 April 1975)

Angular distributions have been obtained at an incident energy of 100 MeV corresponding to $^{32}$S elastic scattering on $^{27}$Al, $^{27}$Al($^{32}$S, $^{31}$P) transitions to the ground and first-excited states of $^{28}$Si and $^{27}$Al($^{32}$S, $^{33}$S) transitions to an unresolved group of low-lying states in $^{26}$Al. An optical model analysis of the elastic data shows that the "best fit" potentials with constant diffusivity follow the $Ve^{R/a}$ = constant ambiguity extremely well. It appears that the elastic data is most sensitive to the ion-ion potential near a radius of $\approx$ 10.1 fm. The absolute cross sections of the $^{27}$Al($^{32}$S, $^{31}$P) transitions to the ground and first-excited states of $^{28}$Si are well reproduced in a distorted-wave Born-approximation analysis using optical model parameters which reproduce elastic scattering. The angular positions of the ($^{32}$S, $^{31}$P) grazing peaks, however, are observed a few degrees forward of their predicted position, and the measured cross sections forward of the grazing peaks are considerably larger than predicted. The agreement between measured and predicted angular shape apparently is better for the $^{27}$Al($^{32}$S, $^{33}$S)$^{26}$Al neutron transfer than for the proton transfer data. From this limited first data for $^{32}$S induced reactions it appears that such reactions can be explained to the extent that "lighter heavy-ion" induced reactions are understood.

[NUCLEAR REACTIONS $^{32}$S + $^{27}$Al elastic scattering; $E$=100 MeV, measured $\sigma(\theta)$; optical model analysis, extracted optical model parameters. $^{27}$Al($^{32}$S, $^{31}$P) and $^{27}$Al($^{32}$S, $^{33}$S); $E$ = 100 MeV, measured $\sigma(\theta)$; DWBA analysis, extracted spectroscopic factors.]

## I. INTRODUCTION

High resolution beams of mass 12–20 nuclei from tandem Van de Graaff accelerators and modern cyclotrons together with improved techniques of particle detection and identification have made possible the study of heavy-ion induced transfer reactions to discrete final states. The proceedings of recent heavy-ion conferences[1] indicate the richness of this rapidly growing research area. The present paper reports an extension of such heavy-ion induced transfer studies to projectiles of $A$ = 32 while sufficient energy and mass resolution is maintained to resolve individual final states. A study of $^{28}$Si induced quasielastic transfer from a target of $^{29}$Si also has been reported previously by Hildenbrand *et al.*[2]

Angular distributions have been measured for the elastic scattering and transfer reactions induced by 100 MeV $^{32}$S incident on an Al target ($\eta \equiv Z_1 Z_2 e^2 m/\hbar^2 k = 18.6$). The elastic scattering is analyzed with a variety of optical model potentials and the differential cross sections of groups corresponding to $^{27}$Al($^{32}$S, $^{31}$P) transitions to the ground and first-excited states of $^{28}$Si are analyzed in terms of the distorted-wave Born approximation (DWBA). This method has been successful in describing most of the properties of $A$ = 12–16 heavy-ion induced single-nucleon transfer reactions (see, e.g., Refs. 3–8).

## II. EXPERIMENTAL METHODS AND RESULTS

A 100 MeV $^{32}$S beam from the Brookhaven National Laboratory Tandem Accelerator Facility was used to study the elastic scattering and the few nucleon transfer reactions induced on a 75 $\mu$g/cm$^2$ self-supporting natural Al foil. Reaction products were detected in a time-of-flight spectrometer[9] consisting of a very thin Pilot-B plastic scintillator[10] start detector and a silicon surface barrier stop detector. The flight path was about 2 m long and the electronic signals from the flight time TAC (time-to-amplitude converter) and the total energy signal from the stop detector were sorted and displayed in a two dimensional 128 × 128 channel format using a Sigma 7 on line computer. The geometry of the spectrometer was arranged so that two separate stop detectors were used with a single start scintillator. This permitted the simultaneous

collection of two spectra each having an angular resolution of ±0.1°(lab) and separated by a laboratory angle of 0.5°. A "typical" two dimensional plot of energy versus time of flight measured at a laboratory angle of 20.5° is shown in Fig. 1. The time resolution is sufficient to distinguish single mass lines up to about mass 40. An energy resolution from the stop counters of ~1 MeV full width at half-maximum was obtained. No charge identification could be derived from the system.

Spectra corresponding to the $A=28$, 30, 31, 32, and 33 mass lines extracted by projection from the data shown in Fig. 1 are shown in Fig. 2. These are the dominant intensities in the mass spectra. Groups identified with the ground state and lowest $2^+$ state at $E_x=1.78$ MeV of $^{28}$Si are labeled on the mass 31 spectra. Contributions corresponding to the excited states of $^{31}$P at 1.27 and 2.23 MeV also may be contained in this latter group although the position and width of this group indicate that it corresponds predominantly to the $2^+$ level of $^{28}$Si.

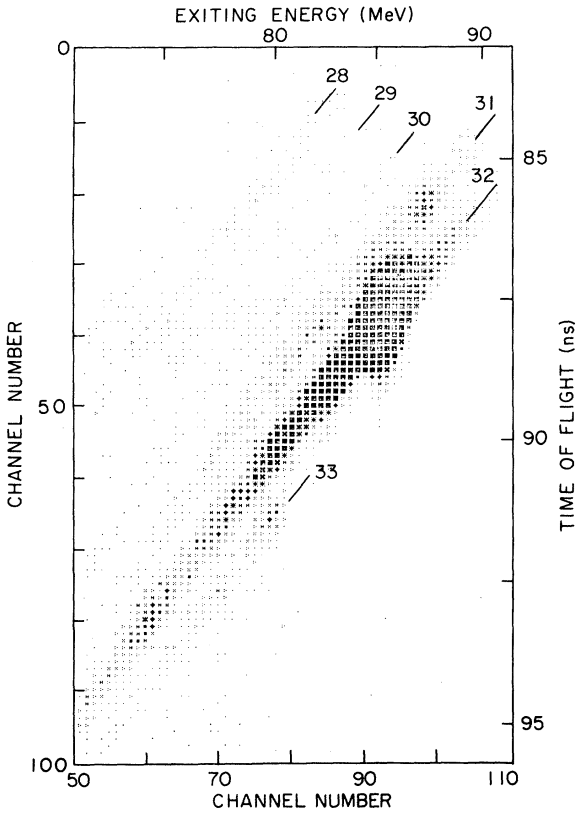


FIG. 1. Plot of energy (abscissa) vs time of flight (ordinate) for the reaction products of 100 MeV $^{32}$S on $^{27}$Al measured at a laboratory angle of 20.5°. Lines of constant masses are indicated, and spectra of those corresponding to $A=28$, 30, 31, 32, and 33 are shown in Fig. 2.

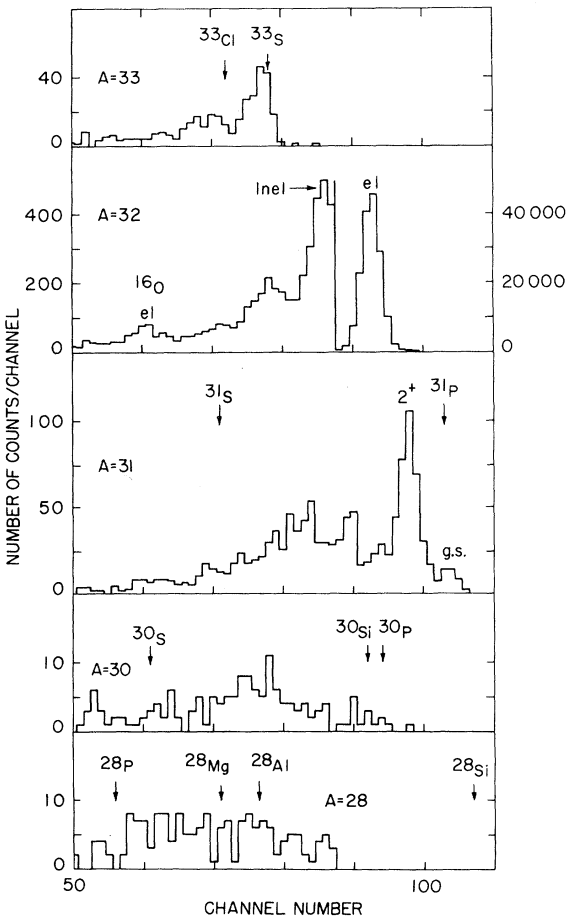


FIG. 2. Mass 28, 30, 31, 32, and 33 energy spectra for 100 MeV $^{32}$S on $^{27}$Al measured at a laboratory angle of 20.5°. These spectra correspond to a portion of that data shown in Fig. 1. The channels corresponding to both the exiting and the residual nuclei being in their ground states are indicated by the arrows labeled with the symbol for the appropriate exiting particle in each spectra. Groups corresponding to the $^{27}$Al($^{32}$S, $^{31}$P) transitions to the ground and first-excited $2^+$ states of $^{28}$Si are indicated in the $A=31$ spectra. The spectra corresponding to the mass groups not shown contain fewer counts at this angle than those shown (see Fig. 1).

The elastic scattering groups from $^{27}$Al and $^{16}$O can be identified in the $A=32$ spectra. A group at channel 86 in this spectrum (labeled "inel") is at the appropriate energy to correspond to an inelastic excitation to either the $\frac{7}{2}^+$ state at 2.21 MeV in $^{27}$Al or to the $2^+$ state at 2.23 MeV in $^{32}$S. The broad group near channel 77 in the mass 33 spectrum is identified with unresolved transitions to the ground states of $^{33}$S and $^{26}$Al and the several low-lying excited states at 0.23, 0.42, and 1.06 MeV in $^{26}$Al and at 0.84 MeV in $^{33}$S.

Angular distributions corresponding to the $^{27}$Al-

($^{32}$S, $^{31}$P) transitions to the ground and first-excited $2^+$ states of $^{28}$Si and to the unresolved $^{27}$Al-($^{32}$S, $^{33}$S)$^{26}$Al transitions are shown in Fig. 3. Two data points separated by 0.5°(lab angle) were obtained as described above every 2.5° in the laboratory between 10 and 30°. The large elastic count rate prevented the measurements of transfer cross sections forward of 10° in the laboratory system. The relative cross sections for the transfer data were obtained by normalizing the elastic scattering measured with the time-of-flight spectrometer to elastic scattering measured separately with a single surface barrier detector (see Fig. 4). The latter data were measured in 0.5–1.0° steps between 7 and 31.5° and was normalized to the sum of two monitor detectors located on opposite sides of the beam. A detector acceptance angle of ±0.075°(lab) was used.

By normalizing to elastic scattering at forward angles where it deviates by <1% from Rutherford an absolute cross section scale was established for both the elastic and transfer data. Because of uncertainties in the absolute angle of the time-of-flight spectrometer arm an over-all uncertainty of ±20% is expected in the absolute cross section scale for the transfer data. The error bars shown with the transfer data in Fig. 3 represent statistical errors as well as uncertainties encountered in separating the mass 31 and 33 lines from the large $A=32$ elastic groups at forward angles. For the elastic scattering uncertainty the quadrature of 1% plus the statistical error was assumed and these errors are shown in Fig. 4 as error bars where they are larger than the signature for data points.

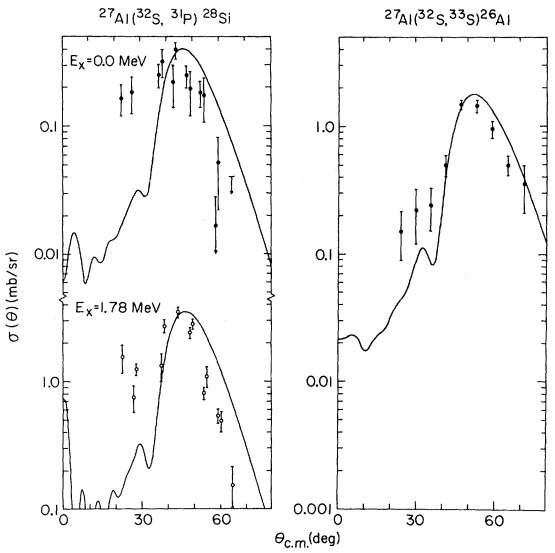


FIG. 3. Angular distributions corresponding to $^{27}$Al-($^{32}$S, $^{31}$P) transitions to the ground and 1.78 MeV states of $^{28}$Si (left side) and to the $^{27}$Al($^{32}$S, $^{33}$S) transitions to the unresolved low-lying states in $^{26}$Al (right side) measured at an incident energy of 100 MeV. The error flags represent statistical errors as well as uncertainties in separating the mass 31 and 33 lines from the larger elastic groups at forward angles. The curves are DWBA predictions calculated using optical model parameter set 100/0.50 of Table I.

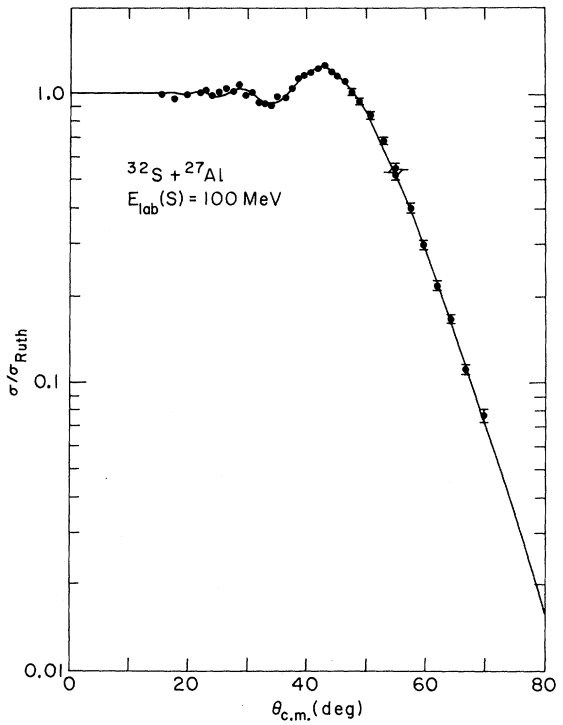


FIG. 4. Elastic scattering data corresponding to 100 MeV $^{32}$S on $^{27}$Al. The errors shown when they are larger than the data points represent the quadrature of 1% and statistical error. The curve was calculated using optical model parameters labeled 100/0.50 in Table I which were obtained by searching on the imaginary well depth $W$ and the channel radius $R \equiv r_0(27^{1/3}+32^{1/3})$. Curves corresponding to nearly identical "fits" to the data are shown in Fig. 5.

## III. ELASTIC SCATTERING ANALYSIS

The 100 MeV $^{32}$S + $^{27}$Al elastic scattering data (see Fig. 4) were analyzed in terms of the phenomenological optical model using the heavy-ion version of the search code[11] ABACUS. A four-parameter complex potential of Woods-Saxon form with identical real and imaginary geometry was employed throughout the analysis:

$$U(r) = -(V+iW)\left[1+\exp\left(\frac{r-R}{a}\right)\right]^{-1} \quad (1)$$

with $R = r_0(A_1^{1/3} + A_2^{1/3})$. The Coulomb radius was fixed equal to the radius $R$. The elastic data were fitted by simultaneously searching on the imaginary potential depth $W$ and the radius $R$ for a variety of real potentials $V$ and diffusivities $a$. The resulting optical model parameters are tabulated in Table I and the predicted elastic scattering of the 100/0.50 potential ($V = 100$ MeV, $a = 0.50$ fm—see Table I for the other parameters) are shown with the experimental data in Fig. 4.

The "best fit" optical potentials obtained for a definite value of $a$ follow the Igo ambiguity[12,13] ($Ve^{R/a} = \text{constant}$) extremely well (see Table I) for the entire range of $V$'s considered (20 MeV $\leq V \leq$ 1000 MeV). Furthermore, the ratio of $W/V$ only changes by ~25% over the range of $V$'s and is nearly independent of the diffusivities used ($0.45 \leq a \leq 0.55$). The potentials in Table I for a definite diffusivity are essentially identical at distances $\gtrsim 10$ fm (see left side of Fig. 5 and Fig. 6). Such potentials generate nearly identical partial-wave scattering amplitudes[14] $\eta_l$ for all partial waves (see left side of Fig. 7), even though the real and imaginary nuclear potentials are very different inside of ≈9 fm. The small differences observed in the phase derivatives $2(\partial\delta/\partial l)$ at the lowest partial waves correspond to amplitudes $|\eta_l|$ which approach zero. Similar approximate invariance of the generated partial-wave amplitudes for widely varying potential depths connected by the "continuous ambiguity" has previously been demonstrated[13] for elastic $\alpha$-particle scattering.

The $Ve^{R/a} = \text{constant}$ ambiguity, however, does not hold between the parameter sets with different diffusivities (see Table I). Potentials for different diffusivities, in spite of the fact that they generate almost identical elastic scattering cross sections, do not have identical tails. Some small differences also are observed in the calculated partial-wave amplitudes with potentials of different diffusivities (see right side of Fig. 7) leading to differences in the predicted large angle elastic scattering cross sections. Such differences were not found with potentials having the same diffusivity (see Fig. 5). The present elastic data do not distinguish between the diffusivities ($0.45 \leq a \leq 0.55$) used in the analysis.

The interaction barrier heights $V_B$, defined to be the maximum of the sum of Coulomb plus real nuclear potential, and the interaction radius $R_B$, the nuclear separation corresponding to the interaction barrier, also are given in Table I. Consistent values of the interaction barriers are predicted using the best fit optical potentials determined from the analysis of elastic data.

It appears from Figs. 5 and 6 that all the potentials of Table I pass through the same point at an ion-ion separation of 10.1 fm. The elastic scattering data thus cannot be claimed to determine the tails of the potentials; only the value at 10.1 fm is determined unambiguously. The classical Rutherford orbit having a turning point distance ($\rho_t$) of 10.1 fm under the present kinematical conditions[15] corresponds to an impact parameter of $p = 6.00$ fm and to a scattering angle of $\theta_{\text{c.m.}} = 57.2°$. [A classical interpretation should be quite accurate here because of the large value of $\eta = 18.6$. Furthermore, $\text{Re}U(10.1\text{ fm}) = 0.5$ MeV compared with $U_{\text{Coul}}(10.1\text{ fm}) \approx 30$ MeV.] It is seen from Fig. 4 that $\theta = 57.2°$ corresponds to a cross section of 0.4 of the Rutherford cross section. This value may be compared with the strong absorption radius $R_c$ which corresponds to a transmission coefficient $T = 1 - |\eta_l|^2 = \frac{1}{2}$. In the strong absorption limit $R_c$ is defined from the orbit corresponding to an elastic cross section of 0.25 of the Ruther-

TABLE I. Optical model parameters obtained from fits to elastic scattering data.

| Parameter set | $V$ (MeV) | $W$ (MeV) | $r_0$ (fm) | $a$ (fm) | $W/V$ | $Ve^{R/a}$ [a] ($10^8$ MeV) | $\chi^2$ | $V_B$ [b] (MeV) | $R_B$ [c] (fm) |
|---|---|---|---|---|---|---|---|---|---|
| 20/0.45 | 20 | 12.02 | 1.361 | 0.45 | 0.601 | 25.8 | 2.67 | 29.9 | 9.5 |
| 100/0.45 | 100 | 48.56 | 1.245 | 0.45 | 0.486 | 26.3 | 2.67 | 29.8 | 9.6 |
| 1000/0.45 | 1000 | 467.7 | 1.078 | 0.45 | 0.468 | 26.6 | 2.73 | 29.8 | 9.6 |
| 20/0.50 | 20 | 12.05 | 1.331 | 0.50 | 0.602 | 2.75 | 2.60 | 30.1 | 9.4 |
| 100/0.50 | 100 | 48.76 | 1.203 | 0.50 | 0.488 | 2.83 | 2.56 | 30.0 | 9.4 |
| 1000/0.50 | 1000 | 468.8 | 1.016 | 0.50 | 0.469 | 2.81 | 2.33 | 30.0 | 9.5 |
| 20/0.55 | 20 | 12.06 | 1.303 | 0.55 | 0.603 | 0.451 | 3.30 | 30.4 | 9.2 |
| 100/0.55 | 100 | 48.82 | 1.161 | 0.55 | 0.488 | 0.458 | 2.86 | 30.2 | 9.3 |
| 1000/0.55 | 1000 | 469.7 | 0.956 | 0.55 | 0.470 | 0.458 | 2.76 | 30.1 | 9.4 |

[a] $R = r_0(27^{1/3} + 32^{1/3})$.
[b] Maximum value of real nuclear plus Coulomb potential.
[c] Radius corresponding to maximum in real nuclear plus Coulomb potential.

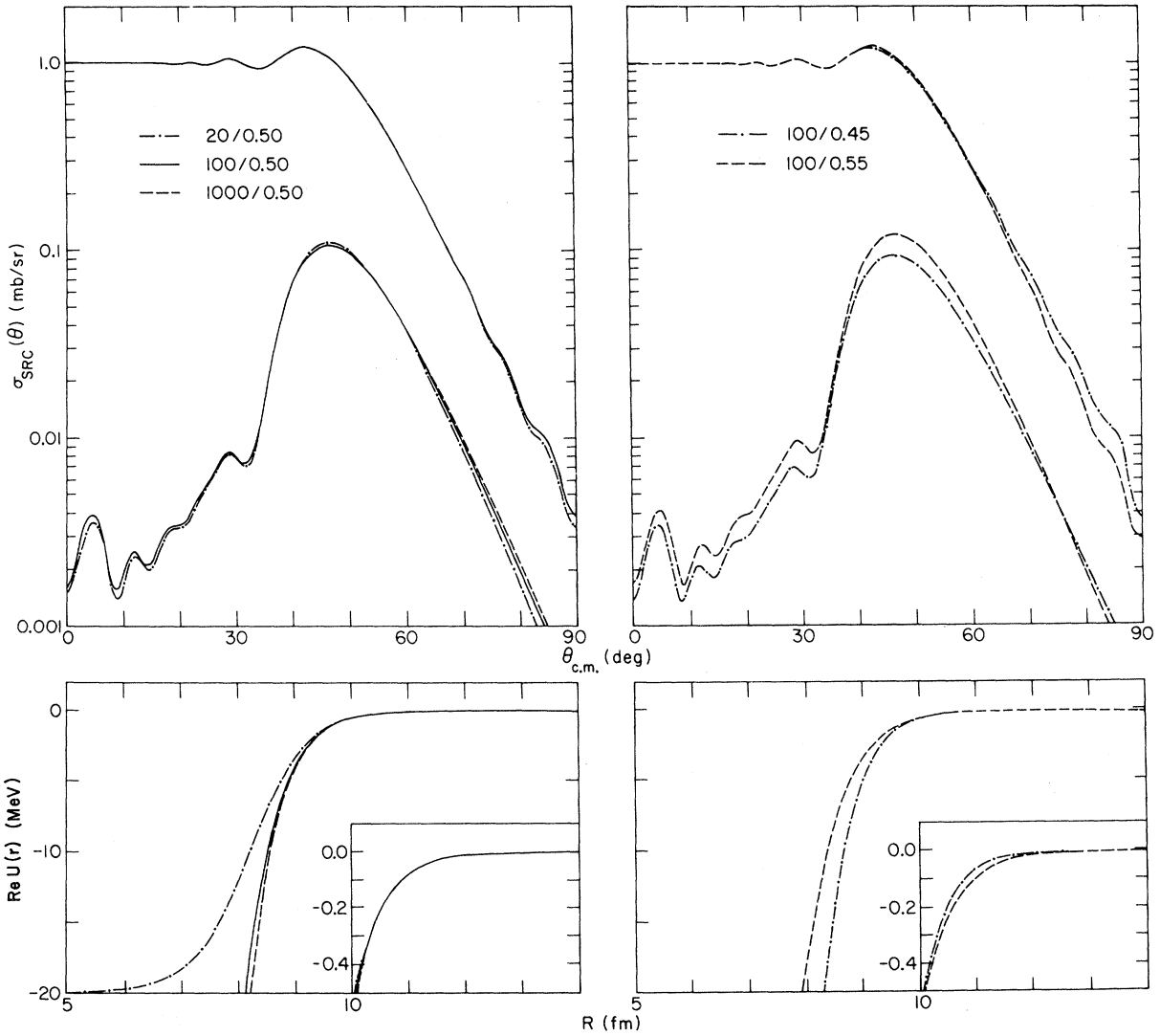


FIG. 5. Comparison of elastic scattering and $^{27}Al(^{32}S,^{31}P)^{28}Si$ ground state transfer cross sections predicted using various best fit optical parameters obtained from fitting elastic scattering data as described in the text. Also shown are the real nuclear potentials as a function of the channel radius. On the left side calculations based on optical parameters (see Table I) with constant diffusivity ($a = 0.50$ fm) and various real well depths ($10 \leq V \leq 1000$ MeV) are shown. On the right similar calculations are shown for constant $V = 100$ MeV and various diffusivities ($0.45 \leq a \leq 0.55$ fm). The calculated elastic scattering and transfer cross sections using the parameter set labeled 100/0.50 shown in this figure are displayed with the experimental data in Figs. 4 and 3, respectively. The elastic scattering calculated using potential sets 100/0.50 and 1000/0.50 are so similar that only one curve is shown.

ford value. The corresponding values of the scattering angle and turning point separation for Rutherford orbits are $\theta = 61°$ and $\rho_t = 9.7$ fm, respectively. Thus the elastic scattering determines the potentials at a separation of about 0.5 fm outside of the strong absorption radius.

In an analysis of the elastic scattering of 72.2 MeV $^{11}B$ from $^{208}Pb$ ($\eta = 25.2$) Satchler[14] found that the potential was unique at a separation corresponding to $\sigma_{el} = 0.3\sigma_R$. This value corresponds to a radius somewhat closer to the strong absorption radius $R_c$ than found in the present study of $^{32}S + ^{27}Al$. It is not clear if any physical significance should be attached[16] to the few tenths of a femtometer larger deviation from $R_c$ for the sensitive radius of the $^{32}S + ^{27}Al$ potential (determined from data at one incident energy) than for potentials of "lighter heavy ions."

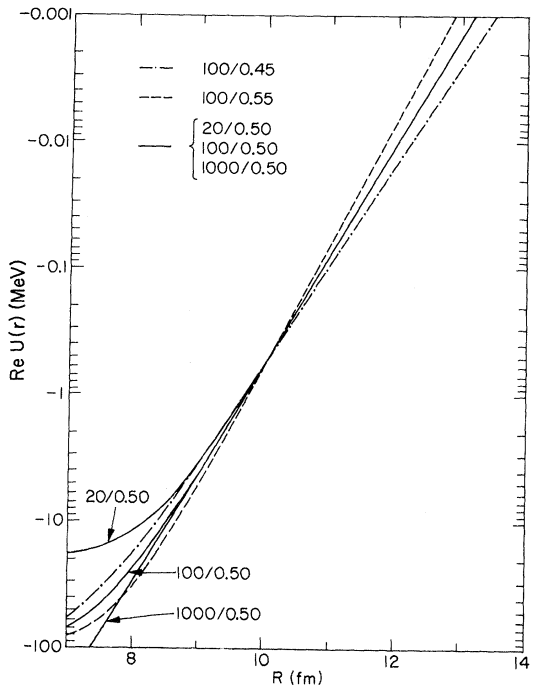


FIG. 6. Log plot of the "best fit" real nuclear potential as a function of the channel radii for some of those potentials given in Table I. The best fit potentials with constant diffusivities are nearly identical for radii $\gtrsim 10$ fm. The potential sets having different diffusivities are identical in magnitude for radii near 10.1 fm only indicating a sensitivity of the elastic scattering to such radii and explaining why larger variations are predicted for elastic scattering and transfer using the potentials of varying diffusivity (see Fig. 5).

## IV. TRANSFER ANALYSIS

The experimental $\sigma_{\text{exp}}(\theta)$ and calculated $\sigma_{\text{SRC}}(\theta)$ single-nucleon transfer cross sections for the reaction $A(a,b)B$ are related through the spectroscopic factors $C^2S$ by

$$\sigma_{\text{exp}}(\theta) = (C^2S)_{ab}(C^2S)_{AB}\sigma_{\text{SRC}}(\theta) \ . \qquad (2)$$

The theoretical differential cross sections $\sigma_{\text{SRC}}(\theta)$ were calculated using the finite-range DWBA code SRC of Baltz.[5,17] The effects of recoil were included using a series expansion[5,18] keeping terms to the second order, which under the present conditions, should be accurate to a few percent.

### A. $^{27}$Al($^{32}$S,$^{31}$P)$^{28}$Si reaction

In ($^{32}$S, $^{31}$P) reactions when the $^{31}$P is produced in its ground state a $2s_{1/2}$ proton is transferred between $^{32}$S and $^{31}$P; therefore, only a single transferred $L$ is allowed for each transition to a particular shell-model orbit. Furthermore, the transferred $L$ is identical to the $l$ of the shell-model orbit which it enters in the residual nucleus, and the $L$ values are the same as for ($^3$He, $d$) or ($d$, $n$) where a $1s_{1/2}$ proton is transferred. The $s_{1/2}$ transfer between projectile and ejectile simplifies the analysis considerably and removes the complication of a non-normal transferred $L$, the result of transverse recoil.[5]

DWBA predictions are shown in Fig. 3 with the angular distributions corresponding to $^{27}$Al($^{32}$S, $^{31}$P) transitions to the ground and first-excited states of $^{28}$Si. The curves shown were calculated using the optical potentials labeled 100/0.50 in Table I, in both entrance and exit channels. These potentials were derived from the elastic scattering analysis—see Sec. III. The bound-state well parameters given in Table II were used in all the DWBA calculations. Nearly identical transfer cross sections are predicted using other optical potentials which fit the elastic scattering (see Fig. 5). This is expected since the ion-ion potentials derived from the elastic scattering data are well determined in the region of ion-ion separations that contribute to the transfer cross section.[19]

The curve shown in Fig. 3 with the $^{27}$Al($^{32}$S, $^{31}$P) transition to the 1.78 MeV $2^+$ excited state of $^{28}$Si corresponds to pure $2s_{1/2}$ proton transfer to the $^{27}$Al $\frac{5}{2}^+$ ground state even though both $d_{3/2}$ and $d_{5/2}$ transfer are allowed. Indeed $d$ strength has been observed[20,21] in the light-ion induced single-proton transfer populating the 1.78 MeV state in $^{28}$Si. DWBA calculations predict nearly identical angular shapes for $2s_{1/2}$ $L=0$ and $1d_{5/2}$ $L=2$ transfer to this state except at the most forward angles where data do not exist. The DWBA cross section corresponding to $2s_{1/2}$ $L=0$ transfer, however, is predicted to be $\approx$4.5 times larger at the grazing peak than the $L=2$ $1d_{5/2}$ transfer, presumably the result of a larger magnitude for the $2s_{1/2}$ bound-state wave function at the nuclear surface as compared to the $1d_{5/2}$ form factor. The magnitude of the predicted transfer with the proton in a $1d_{5/2}$ state in both $^{28}$Si and $^{32}$S for otherwise identical parameters is reduced further by a factor of $\approx$4 because the "tail" of the bound-state wave function is now small in both $^{28}$Si and $^{32}$S. Since the 1.27 and 2.23 MeV states of $^{31}$P have $J^\pi = \frac{3}{2}^+$ and $\frac{5}{2}^+$, respectively, the configuration dependence of the cross sections explains why a strong yield is not observed in the mass 31 spectrum corresponding to $^{31}$P excited to these two states and $^{28}$Si in its ground state. Similarly, the configuration dependence helps[22] to explain why the cross sections to $^{28}$Si($2^+$) is almost an order of magnitude larger than the ground state $^{27}$Al($^{32}$S, $^{31}$P) cross section. Similar configuration dependences have been observed[6,23,24] for transfer induced by "lighter heavy

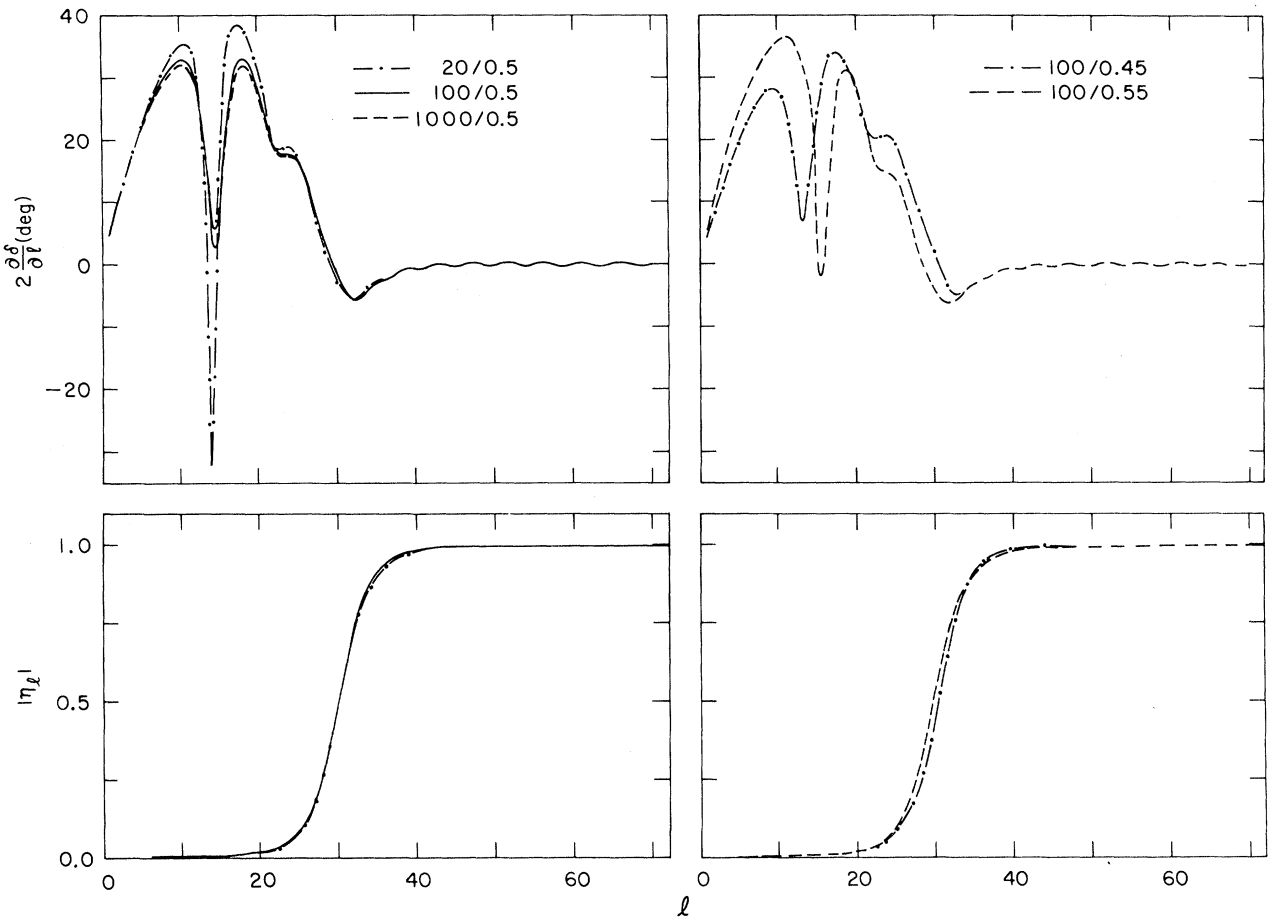


FIG. 7. Absolute value of the scattering amplitude $|\eta_l|$ and phase derivative $2(\partial\delta/\partial l)$ of the elastic nuclear phase as a function of the partial wave $l$ for the potentials compared in Figs. 5 and 6. This figure is laid out similar to Fig. 5 with a comparison of the results for best fit potentials of constant diffusivities and constant real nuclear depth on the right and left, respectively. The amplitudes $|\eta_l|$ for the potential sets 100/0.50 and 1000/0.50 are so similar that only one curve is shown.

ions." In these cases, however, it is not so dramatic, because the least strongly bound nucleon in the projectile-ejectile system does not have a node near the nuclear surface[25] as does the $2s_{1/2}$ form factor.

The DWBA calculations shown with the ($^{32}$S, $^{31}$P) data in Fig. 3 underpredict the experimental cross sections at the most forward angles and overpredict the observed yield at backward angles. Cross sections calculated using the other parameters which fit elastic scattering produce curves essentially identical (see Fig. 5) to that shown with the

TABLE II. Surface transparent potentials used in the DWBA prediction shown in Figs. 9.

| Channel | $V$ (MeV) | $R$ (fm) | $a=a'_{SD}$ (fm) | $W_{WS}$ (MeV) | $W_{SD}$ (MeV) | $R'_{WS}=R'_{SD}$ | $a'_{WS}$ (fm) |
|---|---|---|---|---|---|---|---|
| $^{32}$S + $^{27}$Al | 100 | 7.428 | 0.50 | 100 | 2.5 | 7.10 | 0.10 |
| $^{31}$P + $^{28}$Si | 100 | 7.432 | 0.50 | 100 | 2.5 | 7.10 | 0.10 |
| Bound state [a] | b | $1.25A^{1/3}$ | 0.65 | ... | ... | ... | ... |

[a] Used for all DWBA calculations in this paper.
[b] Varied to give the transferred nucleons the correct binding energy.

data in Fig. 3. Similar problems have been observed in proton transfer induced by "lighter heavy ions" (see e.g., Refs. 3, 6, 7, 23, 24, 26, and 27). An *ad hoc* solution for the problem is modifying[3,27] the optical model potentials to reproduce the data. Weakened absorption near the nuclear surface will change the predicted shape of the angular distribution in the correct direction (see Fig. 8). The surface transparent potentials[8,28] used in this calculation are given in Table II. Such weakly absorbing potentials, however, no longer reproduce the elastic data (Fig 9). An exactly analogous situation has been reported for the $^{27}$Al($^{16}$O, $^{15}$N)$^{28}$Si reaction in Ref. 29. It is quite possible that transfer reactions from a near deformed nucleus such as $^{27}$Al require a more sophisticated analysis than is provided by the DWBA in order to obtain a detailed agreement between experiment and theory. Changes in the optical model parameters away from those that fit elastic scattering can to some extent compensate for the neglect of coupled channel effects.[27]

The spectroscopic factors for proton transfer to $^{27}$Al obtained from the DWBA analysis of the $^{27}$Al-($^{32}$S, $^{31}$P)$^{28}$Si reaction are compared in Table III with values from studies of the $(d,n)$[20] and ($^3$He, $d$)[21] reactions on $^{27}$Al. The tabulated ($^{32}$S, $^{31}$P) spectroscopic factors assume a spectroscopic factor of 1.4 for the removal of a proton from $^{32}$S

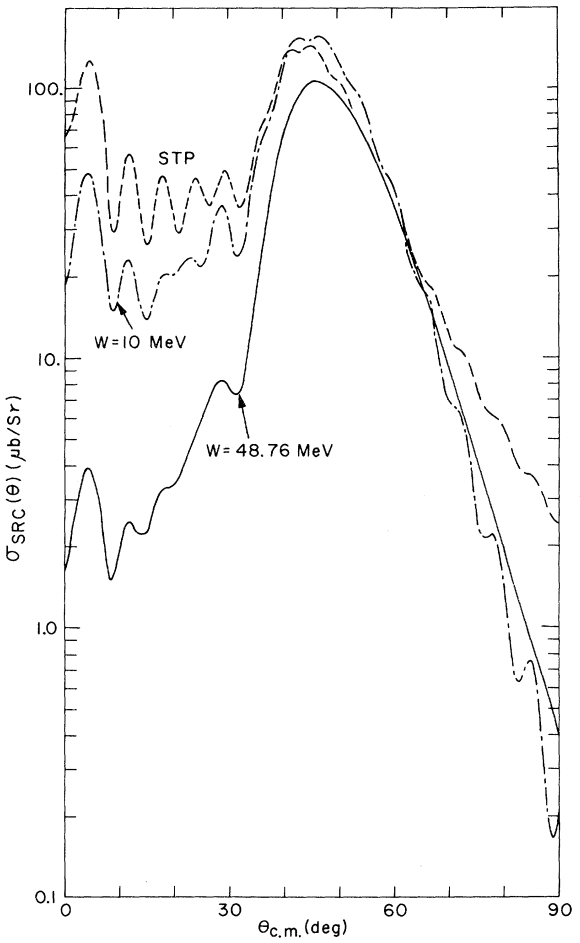


FIG. 8. Comparison of predicted differential cross sections for the $^{27}$Al($^{32}$S, $^{31}$P) transition to the $^{28}$Si ground state using optical model potentials differing only in the imaginary part. The solid curve labeled $W$=48.76 MeV corresponds to potential set 100/0.50 of Table I and is shown with the transfer data in Fig. 3. The dash-dot curve corresponds to set 100/0.50 with the imaginary depth reduced to $W$=10 MeV, and the dashed curve corresponds to the surface transparent potentials (STP) given in Table II and similar to the potentials discussed in Refs. 8 and 28. The potentials having weaker absorption near the nuclear surface reproduce the cross sections forward of the grazing angle better; however, such potentials fail to reproduce the elastic scattering of $^{32}$S on $^{27}$Al—see Fig. 9.

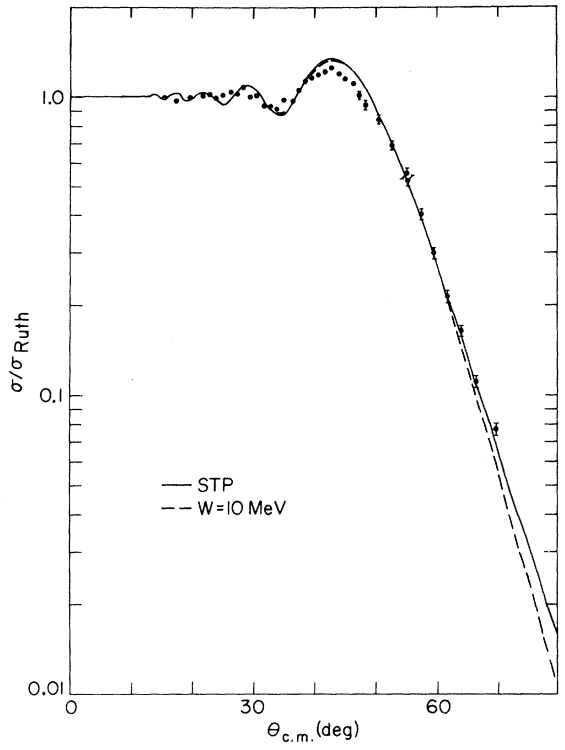


FIG. 9. Comparison of predicted elastic scattering calculated with the potentials which are weaker in the region of the nuclear surface and the elastic data. Such potentials fail to reproduce the elastic scattering particularly near the "glory peak." The transfer cross section based on such potentials are compared in Fig. 8 to optical model set 100/0.50 of Table I which fits the elastic data. See caption of Fig. 8 for a description of the potential used in the calculations for this figure.

TABLE III. Comparison of spectroscopic factors derived from $^{27}$Al($^{32}$S, $^{31}$P)$^{28}$Si and light-ion induced transfer.

| $E_x$ in $^{28}$Si (MeV) | $J^\pi$ | $L, j_p$ [a] | $\sigma_{exp}/\sigma_{SRC}$ [b] | $C^2S(^{27}\text{Al}+p\rightarrow{}^{28}\text{Si})$ $(^{32}\text{S}, ^{31}\text{P})$ [c] | $(d, n)$ [d] | $(^3\text{He}, d)$ [e] |
|---|---|---|---|---|---|---|
| 0.0 | $0^+$ | $2, \frac{5}{2}$ | 3.8 | 2.7 | 1.5 | 2.6 |
| 1.78 | $2^+$ | $0, \frac{1}{2}$ | 0.80 [f] | 0.57 [f] | 0.19 | 0.46 |
| | | $2, \frac{5}{2}$ | f | f | 0.08 | 0.08 |

[a] Transferred $L$ and spin of particle transferred to $^{27}$Al.
[b] Corresponds to fits shown in Fig. 3.
[c] Assuming $C^2S=1.4$ for $^{32}\text{S}\rightarrow{}^{31}\text{P}+p$. See Ref. 30.
[d] Reference 20.
[e] Reference 21.
[f] Because the $L=0$ predicted cross section is ~4.5 times larger than the $L=2$ cross section and the light-ion transfer results indicate that this transition is predominately $s_{1/2}$ transfer, the $C^2S$ extracted from the present study assumes pure $L=0$ transfer. Assuming $C^2S=0.08$, the value from light-ion transfer, for the $L=2$ transfer would reduce the extracted $L=0$ $^{27}$Al-($^{32}$S, $^{31}$P)$^{28}$Si spectroscopic factor for this state by only 3%.

leaving $^{31}$P in its ground state.[30] The spectroscopic factors extracted from the present analysis are in excellent agreement with those obtained from an $^{27}$Al($^3$He, $d$)$^{28}$Si study.[21] The factor of 10 variation in the differential cross sections for the $^{27}$Al-($^{32}$S, $^{31}$P) transitions to the ground and first-excited states of $^{28}$Si is explained by the DWBA analysis.

### B. $^{27}$Al($^{32}$S,$^{33}$S)$^{26}$Al reaction

The right hand side of Fig. 3 shows the angular distribution of a broadened group in the mass 33 spectra (Fig. 2) associated with unresolved $^{27}$Al-($^{32}$S, $^{33}$S)$^{26}$Al transition to the ground states of $^{33}$S and $^{26}$Al and the low-lying excited states at 0.23, 0.42, and 1.06 MeV in $^{26}$Al and at 0.84 MeV in $^{33}$S. The curve shown with the data corresponds to the angular shape predicted for the $^{27}$Al($^{32}$S, $^{33}$S)$^{26}$Al transition with both $^{33}$S and $^{26}$Al in their ground states. The angular shapes for the other transitions which may contribute to this group are nearly identical to that shown except at the forward-most angles where data do not exist. This predicted curve is arbitrarily normalized to the data. No attempt has been made to extract spectroscopic information, since so many unresolved transitions can contribute to this angular distribution. The agreement between the predicted and observed angular shape for the ($^{32}$S, $^{33}$S) group, however, probably is better than observed in the analysis of the ($^{32}$S, $^{31}$P) single-proton transfer.

## V. CONCLUSIONS

The relative and absolute "grazing peak" cross sections for the $^{27}$Al($^{32}$S, $^{31}$P)$^{28}$Si transitions observed were reproduced in a finite range DWBA analysis including recoil corrections. The angular positions of the $^{27}$Al($^{32}$S, $^{31}$P)$^{28}$Si grazing peaks, however, are observed a few degrees forward of their predicted positions, and the measured cross sections forward of the graxing peak apparently are considerably larger than predicted (see Fig. 3). By weakening the absorption at the nuclear surface the angular shape of the $^{27}$Al($^{32}$S, $^{31}$P)$^{28}$Si cross section can be reproduced; however, such optical potentials no longer reproduce the elastic scattering. From the limited $^{27}$Al($^{32}$S, $^{33}$S)$^{26}$Al neutron transfer data it appears that the agreement between predicted and measured angular shapes may be better for neutron transfer than for proton transfer.

The analysis of the elastic data indicates that the optical potentials which reproduce the elastic data follow the $Ve^{R/a}$ = constant ambiguity for potentials with the same diffusivity over a large range of $V$. Such ambiguous potentials produce nearly identical partial wave scattering amplitudes $\eta_l$ for all partial waves. The elastic scattering of 100 MeV $^{32}$S on $^{27}$Al unambiguously determines the real nuclear potential at a distance of about 10.1 fm which is about 0.5 fm larger than the strong absorption radius of 9.7 fm.

The authors wish to acknowledge informative conversations with A. J. Baltz and R. C. Fuller.

†Work performed under the auspices of the Energy Research and Development Administration.

*Permanent affiliation: Niels Bohr Institute, University of Copenhagen, 2100 Copenhagen, Denmark.

[1]Proceedings of the Symposium on Heavy Ion Reactions and Many Particle Excitations, Saclay, [J. Phys. (Paris) Suppl. 32, C6 (1971)]; Proceedings of European Conference on Nuclear Physics, Aix-en-Provence, 1972 [J. Phys. (Paris) Suppl. 33, C5 (1972); Proceedings of the Symposium on Heavy-Ion Transfer Reactions, Argonne National Laboratory, 1973, ANL Informal Report No. Phys. 1973B; *Proceedings of the International Conference on Reactions between Complex Nuclei, Nashville, 1974,* edited by R. L. Robinson *et al.* (North-Holland, Amsterdam/American Elsevier, New York, 1974), Vols. I and II; *Proceedings of the Symposium on Classical and Quantum Mechanical Aspects of Heavy Ion Collisions, Heidelberg, Germany, October, 1974,* edited by H. L. Harney *et al.* (Springer-Verlag, Berlin, 1975).

[2]K. D. Hildenbrand, R. Bock, H. G. Bohlen, P. Braun-Munzinger, D. Fick, C. K. Gelbke, W. von Oertzen, and W. Weiss, Phys. Lett. 42B, 425 (1972).

[3]J. L. C. Ford, Jr., K. W. Toth, G. R. Satchler, D. C. Hensley, L. W. Owen, R. M. DeVries, R. M. Gaedke, P. J. Riley, and S. T. Thornton, Phys. Rev. C 10, 1429 (1974).

[4]P. D. Bond, J. D. Garrett, O. Hansen, S. Kahana, M. J. LeVine, and A. Z. Schwarzschild, Phys. Lett. 47B, 231 (1973).

[5]J. S. Blair, R. M. DeVries, K. G. Nair, A. J. Baltz, and W. Reisdorf, Phys. Rev. C 10, 1856 (1974).

[6]D. G. Kovar, in *Proceedings of the International Conference on Reactions between Complex Nuclei, Nashville, 1974* (see Ref. 1), Vol. II, p. 235.

[7]D. K. Scott, in *Proceedings of the Symposium on Classical and Quantum Mechanical Aspects of Heavy Ion Collisions, Heidelberg, Germany, October, 1974* (see Ref. 1), p. 165.

[8]J. D. Garrett, in *Proceedings of the Symposium on Classical and Quantum Mechanical Aspects of Heavy Ion Collisions, Heidelberg, Germany, October, 1974* (see Ref. 1), p. 59.

[9]T. M. Cormier, R. S. Galik, E. R. Cosman, and A. J. Lazzarini, Nucl. Instrum. Methods 119, 145 (1974).

[10]Product of Nuclear Enterprises, San Carlos, Calif.

[11]E. H. Auerbach (unpublished).

[12]G. Igo, Phys. Rev. Lett. 1, 72 (1958); Phys. Rev. 115, 1665 (1959).

[13]J. S. Blair, in *Proceedings of the International Conference on Nuclear Reactions Induced by Heavy Ions, Heidelberg, Germany, 1969,* edited by R. Bock and W. R. Hering (North-Holland, Amsterdam, 1970), p. 1.

[14]G. R. Satchler, in *Proceedings of the International Conference on Reactions between Complex Nuclei, Nashville, 1974,* (see Ref. 1), Vol. II, p. 171.

[15]We have here used the standard classical trajectory formulas $\rho_t = a[\mathrm{cosec}(\frac{1}{2}\theta)+1]$, $\tan(\frac{1}{2}\theta) = a/p = \eta/(L+\frac{1}{2})$ with $a = 1.44(z_1 z_2)/2E_{\mathrm{lab}}(1+A_1/A_2)$ and $L+\frac{1}{2} = kp$ where $k$ is the wave number. For $\rho_t = 10.1$ fm we find $L = 33.6$ using $k = 5.67$ fm$^{-1}$.

[16]The fact that $^{32}$S and $^{27}$Al are deformed or at least soft toward deformation has been ignored in these discussions, since the inelastic cross section is at most a few percent of the elastic cross section. Thus the neglect of coupled channel effects in the elastic channel probably is not serious.

[17]A. J. Baltz, in *Proceedings of the International Conference on Reactions between Complex Nuclei, Nashville, 1974* (see Ref. 1), Vol. I, p. 60.

[18]A. J. Baltz and S. Kahana, Phys. Rev. C 9, 2243 (1974).

[19]The important radial region for transfer was determined to be 9.5–11.5 fm corresponding to the lower radial integration cutoff on the DWBA calculation for which the total cross section decreases from 90% to 10% of its value for no cutoff. It is noted that the radii so determined to contribute in $^{27}$Al($^{32}$S, $^{31}$P) transfer are outside the radius at which the Coulomb and nuclear forces balance (see Table I) in contrast to transfer reactions induced with lighter ions (see e.g. Ref. 8). No significant differences are observed in the sensitive radii for $2s_{1/2}$ and $1d_{5/2}$ transfer between the projectile and ejectile even though the $2s_{1/2}$ bound-state wave function has a larger magnitude in the nuclear surface region.

[20]W. Bohne, H. Fuchs, K. Grabisch, M. Hagen, H. Homeyer, U. Janetzki, H. Lettau, K. H. Maier, H. Morganstern, P. Pietrzyk, G. Roschert, and J. A. Scheer, Nucl. Phys. A131, 273 (1969).

[21]R. W. Barnard and G. D. Jones, Nucl. Phys. A108, 641 (1968).

[22]There also is a $2J_f+1$ statistical factor which enters the calculated cross sections $\sigma_{\mathrm{SRC}}(\theta)$ which also favors the $2^+$ state.

[23]D. G. Kovar, B. G. Harvey, F. D. Becchetti, J. Mahoney, D. L. Hendrie, H. Homeyer, W. von Oertzen, and M. A. Nagarajan, Phys. Rev. Lett. 30, 1075 (1973).

[24]F. D. Becchetti, D. G. Kovar, B. G. Harvey, D. L. Hendrie, H. Homeyer, J. Mahoney, W. von Oertzen, and N. K. Glendenning, Phys. Rev. C 9, 1543 (1974).

[25]This is not true however for single-nucleon transfer involving $^{19}$F or $^{19}$Ne as projectiles or ejectiles since these nuclei have $\frac{1}{2}^+$ ground states.

[26]R. H. Siemssen, C. L. Fink, L. R. Greenwood, and H. J. Korner, Phys. Rev. Lett. 28, 626 (1972).

[27]T. Tamura and K. S. Low, Phys. Rev. Lett. 48B, 285 (1974).

[28]P. D. Bond, J. D. Garrett, S. K. Kahana, M. J. LeVine, and A. Z. Schwarzschild, in *Proceedings of the International Conference on Reactions between Complex Nuclei, Nashville, 1974* (see Ref. 1), Vol. I, p. 54; and A. J. Baltz, P. D. Bond, J. D. Garrett, and S. Kahana, Phys. Rev. C 12, 136 (1975).

[29]J. B. Ball, O. Hansen, J. S. Larsen, D. Sinclair, and F. Videbaek, Nucl. Phys. A244, 341 (1975).

[30]Obtained by renormalizing $^{32}$S($d$, $^3$He) experimental spectroscopic factors to a sum of 2.0 for the $s$ strength. Data is from G. Th. Kaschl, D. Mairle, U. Schmidt-Rohr, and G. J. Wagner, Nucl. Phys. A136, 286 (1969).